SPINTRONICS

Subterahertz spin pumping from an insulating antiferromagnet

Priyanka Vaidya[1], Sophie A. Morley[2], Johan van Tol[3], Yan Liu[4], Ran Cheng[5], Arne Brataas[6], David Lederman[2], Enrique del Barco[1]*

Spin-transfer torque and spin Hall effects combined with their reciprocal phenomena, spin pumping and inverse spin Hall effects (ISHEs), enable the reading and control of magnetic moments in spintronics. The direct observation of these effects remains elusive in antiferromagnetic-based devices. We report subterahertz spin pumping at the interface of the uniaxial insulating antiferromagnet manganese difluoride and platinum. The measured ISHE voltage arising from spin-charge conversion in the platinum layer depends on the chirality of the dynamical modes of the antiferromagnet, which is selectively excited and modulated by the handedness of the circularly polarized subterahertz irradiation. Our results open the door to the controlled generation of coherent, pure spin currents at terahertz frequencies.

In the absence of external magnetic fields and below their Néel ordering temperatures, antiferromagnetic (AF) systems exhibit magnetic order with zero net magnetization (*1*). Unlike ferromagnets, AF materials do not produce stray magnetic fields, and therefore AF elements can be tightly packed while operating independently without cross-talk. AF elements also have a low magnetic susceptibility and thus are immune to external magnetic perturbations. Another salient advantage of AF materials compared with ferromagnetic systems is that in ferromagnets spin dynamics is governed by external, dipolar, and anisotropy fields (typically limited to gigahertz frequencies), whereas in AF materials spin dynamics depends on the combined effect of magnetic anisotropy and the substantial exchange interaction, which leads to spin excitations in the much higher terahertz frequency range. This exchange amplification phenomenon allows for the control of ultrafast AF dynamics with moderate external currents (*2*, *3*), making antiferromagnets an appealing choice for the generation, detection, and modulation of coherent terahertz signals (*4*–*6*). Historically, the terahertz region of the electromagnetic spectrum has been difficult to exploit (*7*).

For decades, AF systems have been an auxiliary element in spintronic devices such as the passive exchange bias layer in spin valves (*8*). Although a few reports of AF anisotropic magnetoresistance have shown that AF materials could be employed to store magnetic information (*3*, *9*–*12*), whether they can be used as active ingredients directly controllable through electrical currents remains unknown. Recently, there has been progress in this direction, owing to the experimental realizations (*11*, *13*, *14*) of spin-orbit torques in AF systems with special lattice symmetries (*15*). Moreover, it has been demonstrated that insulating AF hematite (α-Fe_2O_3) supports long-range spin transport across micrometers (*16*). Nevertheless, a crucial missing piece is the experimental observation of spin-transfer torque (*17*, *18*) and its reciprocal effect, dynamical spin pumping (*19*), which are fundamental to manipulation of the AF order parameter by electrical means. Ross *et al.* reported experiments in an AF (MnF_2/Pt) heterostructure showing a small difference of the inverse spin Hall effect signals upon reversal of the magnetic field, which was consistent with but not specific to coherent spin pumping (*20*).

In this study, we demonstrate subterahertz dynamical generation and injection of pure spin currents—coherent spin pumping—from a crystalline MnF_2 AF insulator layer into a heavy-metal platinum thin film, where strong spin-orbit coupling enables spin-charge current interconversion through the inverse spin Hall effect (ISHE).

Antiferromagnetic resonance in insulating antiferromagnet MnF_2

Below the Néel temperature T_N, the long-range magnetic order in simple colinear AF systems such as uniaxial insulating MnF_2 results from the exchange interaction that favors antiparallel alignment between neighboring sublattice magnetizations ($\vec{M}_1$ and $\vec{M}_2$). In contrast to observations in ferromagnets, the total magnetization $\vec{M} = \vec{M}_1 + \vec{M}_2$ vanishes, and the AF order parameter is represented by $\vec{L} = \vec{M}_1 - \vec{M}_2 \neq 0$, known as the Néel vector (*1*). According to the theories of Kittel (*21*) and Nagamiya *et al.* (*22*), the resonance frequencies of the uniform precessional modes (with wave vector $\mathbf{k} = 0$) are

$$\omega_{res} = \gamma\mu_0\sqrt{2H_A H_E} \pm \gamma\mu_0 H \text{ for } H < H_{SF} \quad (1)$$

$$\omega_{res} = \gamma\mu_0\sqrt{H^2 - 2H_E H_A} \text{ for } H > H_{SF} \quad (2)$$

where γ is the gyromagnetic ratio; H is the external magnetic field applied along the easy (anisotropy) axis; H_A and H_E are the effective fields associated with the uniaxial anisotropy and the AF exchange interaction, respectively; and μ_0 is the permeability of free space. The so-called spin-flop (SF) field, $H_{SF} = \sqrt{2H_E H_A}$, separates the AF dynamics into two distinct regimes. For $H < H_{SF}$, Eq. 1 describes the frequencies of the two dynamical modes exhibiting opposite chiralities, which are split by a longitudinal magnetic field H into a high-frequency mode (HFM) and a low-frequency mode (LFM). As illustrated in the upper right inset of Fig. 1, the high-frequency (low-frequency) mode has right-handed (left-handed) chirality with respect to the magnetic field, a large precessional cone angle for $\vec{M}_1(\vec{M}_2)$, and a spin-down (spin-up) angular momentum. The frequency separation of the two modes increases linearly with an increasing applied field until a sufficiently strong field ($H = H_{SF}$) renders the ground-state configuration unstable. At this critical point, the sublattice magnetic moments abruptly flop toward the normal plane of H and both are canted toward H, so that $\vec{L}$ becomes perpendicular to the anisotropy axis. If the applied field is not perfectly aligned with the easy axis, the SF transition broadens into a finite window in which the HFM drops rapidly with an increasing H (as can be observed in Fig. 1). The resonance frequency in the $H > H_{SF}$ regime [often referred to as the quasi-ferromagnetic mode (QFM)] grows with an increasing H, as shown in Eq. 2. In accordance with the above description, we categorize the dynamical modes in an AF system into three characteristic regimes: (i) the low- and high-frequency modes with opposite chiralities for $H < H_{SF}$, (ii) the SF mode residing in the narrow window of the SF transition, and (iii) the QFM mode for $H > H_{SF}$ [after the SF transition is completed (*23*)].

We computed the magnetization dynamics for each magnetic sublattice of a uniaxial antiferromagnet MnF_2 by solving the Landau-Lifshitz equation

$$\frac{d\vec{M}_i}{dt} = -\mu_0\gamma\vec{M}_i \times \vec{H}_{eff} - \alpha\frac{\mu_0\gamma}{M_s}\left(\vec{M}_i \times (\vec{M}_i \times \vec{H}_{eff})\right) \quad (3)$$

[1]Department of Physics, University of Central Florida, Orlando, FL 32765, USA. [2]Department of Physics, University of California Santa Cruz, Santa Cruz, CA 95064, USA. [3]National High Magnetic Field Laboratory, Florida State University, Tallahassee, FL 32310, USA. [4]College of Sciences, Northeastern University, Shenyang, Liaoning, China. [5]Department of Electrical and Computer Engineering and Department of Physics and Astronomy, University of California, Riverside, CA 92521, USA. [6]Center for Quantum Spintronics, Department of Physics, Norwegian University of Science and Technology, NO-7491 Trondheim, Norway.
*Corresponding author. Email: delbarco@physics.ucf.edu

with an effective field $\vec{H}_{\text{eff}}$ comprising the exchange field ($\mu_0 H_E$ = 47.05 T), the anisotropy field ($\mu_0 H_A$ = 0.82 T), the externally applied field (H), and the microwave field [$\vec{H}_m = (H_o\cos(2\pi f t),\ H_o\sin(2\pi f t + \theta), 0)$], where the polarization is determined by changing the phase factor θ from 0 to 2π, and i = 1, 2 labels the two sublattices. We used the following parameter values for the calculation: $\gamma = \gamma_e$, saturation magnetization M_s = 47.7 kA/m, and α = 0.001, in agreement with previously reported values (*24*, *25*). The theoretical results are displayed in Fig. 1, together with the measured spectroscopic antiferromagnetic resonance (AFMR) absorptions; the experimental data are represented by solid symbols corresponding to three different samples studied at four available frequencies (horizontal orange arrows). Figure S1 shows the corresponding spectra. The upper left inset to Fig. 1 shows the electron paramagnetic resonance (EPR) spectrum obtained at frequency f = 395 GHz (red curve) for the magnetic field range corresponding to the HFM resonance (blue triangle at $\mu_0 H$ = 4.70 T). The EPR signal is markedly distorted by saturation of the probe, owing to the large thickness of the MnF_2 single crystal used in these experiments, but still allows us to determine the location of the resonances spectroscopically (*26*). The results agree well with the theoretical calculations and are in excellent agreement with previously published AFMR data (*25*, *27*) and theoretical analyses (*1*, *22*) reported for MnF_2.

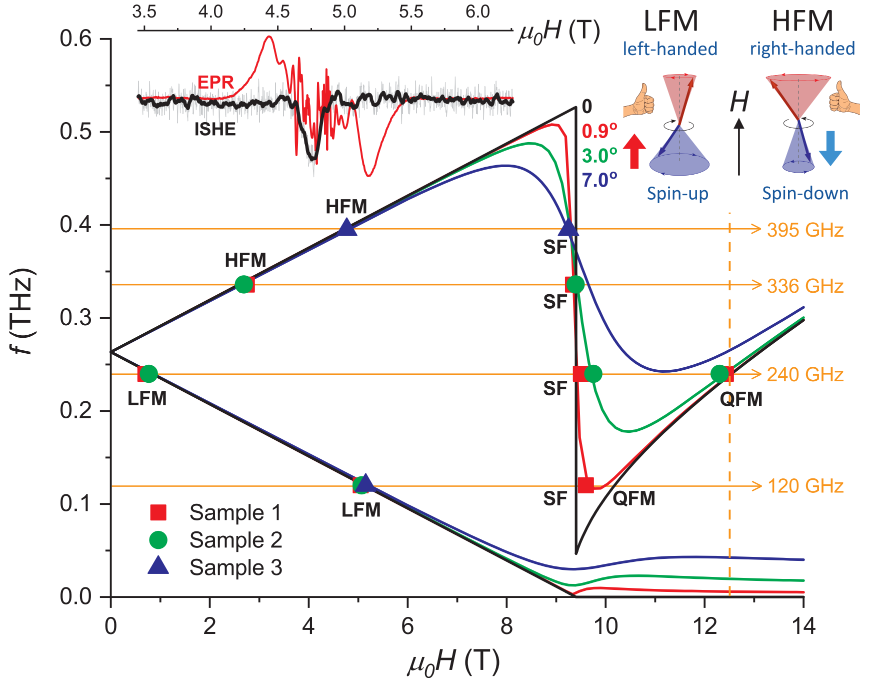

Fig. 1. Antiferromagnetic resonance of MnF_2. Positions of the EPR spectroscopy resonances of MnF_2. The solid curves are the computed resonance frequencies associated with the low- and high-frequency AF modes (upper right inset), the SF transition (at $\mu_0 H_{SF}$~9.4 T), and the QFM at high fields. We use the fitting parameters $\mu_0 H_A = 0.82$ T and $\mu_0 H_E = 47.05$ T in Eq. 1. The different colors correspond to different orientations of the applied magnetic field with respect to the easy anisotropy axis of MnF_2 for each sample. The black curve represents the expected behavior with the field parallel to the easy axis. (Upper left inset) AFMR spectrum (red) and ISHE response (black) in the adjacent platinum layer corresponding to the high-frequency mode resonance at 395 GHz for sample 3 (blue triangle at $\mu_0 H = 4.7$ T).

Coherent spin pumping and the inverse spin Hall effect in MnF_2/Pt

Coherent spin pumping (*28*–*31*) has been central to the advance of ferromagnetic-based spintronics; it serves as a tool to generate spin currents dynamically, avoiding, for example, conductance mismatch issues at the interface between magnetic and nonmagnetic materials. In the realm of AF-based spintronics, Cheng *et al.* developed a theoretical framework to understand dynamical spin injection from an AF material undergoing coherent precession (AFMR) into an adjacent nonmagnetic material (*19*) [see also (*32*)]. Contrary to the conventional wisdom that spin pumping from antiparallel sublattice spins would cancel out, Cheng *et al.* (*19*) established that coherent resonant rotations of different sublattice spins contribute constructively to the pumped spin current. A heuristic understanding of AF spin pumping is that spin currents pumped from the two sublattice magnetization are proportional to $\vec{M}_1 \times \dot{\vec{M}}_1$ and $\vec{M}_2 \times \dot{\vec{M}}_2$, respectively, if we view $\vec{M}_1$ and $\vec{M}_2$ as two independent ferromagnets. As illustrated in Fig. 1 (upper right inset), the two sublattices rotate in the same angular direction with a 180° phase difference; thus, $\vec{M}_1 \approx -\vec{M}_2$ and $\dot{\vec{M}}_1 \approx -\dot{\vec{M}}_2$. Consequently, contributions from the two sublattices add up, yielding a total pumped spin current proportional to $\vec{L} \times \dot{\vec{L}} + \vec{M} \times \dot{\vec{M}}$. Because $H_E \gg H_A$ in MnF_2, we have $|\vec{L}| \gg |\vec{M}|$, and $\vec{M}$ can be approximately expressed in terms of $\vec{L}$ as $\vec{M} \approx \left[\frac{H}{H_E}\vec{L} \times (\hat{z} \times \vec{L}) - \frac{1}{\gamma\mu_0 H_E}\vec{L} \times \dot{\vec{L}}\right]$ (*33*), from which one can tell that $\vec{L} \times \dot{\vec{L}}$ is much larger than $\vec{M} \times \dot{\vec{M}}$. That is to say, it is the Néel vector $\vec{L}$, rather than the vanishingly small magnetization $\vec{M}$, that generates the most essential part of coherent spin pumping. Furthermore, it was predicted in (*19*) that the polarization of the driving ac field determines the direction of the pumped spin current. Dynamical modes with opposite chirality coexist in a colinear AF system at zero field and can be selectively excited by an ac field with matching polarization. In other words, spins are pumped with opposite polarizations depending on whether the right- or left-handed mode is excited (by a right- or left-handed circularly polarized stimulus). A magnetic field breaks the degeneracy between the opposite chirality modes. Consequently, only the correct combination of the irradiation frequency and handedness excites a particular AF mode. Therefore, depending on the handedness of the circular polarization and the frequency of irradiation at a given magnetic field, opposite spin currents would be generated in the adjacent nonmagnetic material and transform into opposite ISHE electric signals.

In the following text, we discuss the measurements of the electrical signals observed by sweeping the magnetic field while irradiating MnF_2/Pt samples with circularly polarized subterahertz microwaves of frequency f. The measured ISHE spectra in samples 3 and 2 are shown in Fig. 2, A and B (f = 395 GHz), and Fig. 2, C and D (f = 240 GHz), respectively. Figure S2 shows the power dependence data for f = 395 GHz. For f = 240 GHz, clear voltage signals were observed associated with the spectra for the LFM, the SF mode, and the QFM. All signals reversed sign when the applied magnetic field reversed direction, which is consistent with the time-reversal symmetry. However, the signal magnitudes differed for opposite handedness of the microwave stimuli, suggesting that chiral AF modes were selectively excited according to the circular polarization. This contrasting magnitude becomes more pronounced in Fig. 2, C and D, where the LFM appears only at a positive (negative) field ($\mu_0|H| = 0.80$T) for the left-handed (right-handed) irradiation. This is indeed the expected behavior of a circularly polarized AF mode in the presence of an external magnetic field. For positive (negative) fields, the LFM mode's chirality is left-handed (right-handed), as it has a spin angular momentum parallel to the magnetic field, whereas the opposite is true for the HFM. There is also a noticeable difference in the strength of the SF signals when only the magnetic field or only the circular polarization is reversed. On the other hand, the magnitude of the QFM resonance remains nearly constant, which we will discuss further in the following text.

Coherent spin pumping versus incoherent spin Seebeck effect

A central question arises from these observations: Do the voltage signals originate from coherent spin pumping at the MnF_2/Pt interface or the incoherent spin Seebeck effect (*34*, *35*) induced by a temperature gradient resulting from microwave heating? In ferromagnets, this is a challenging question because only the right-handed mode exists; therefore, both coherent and incoherent contributions have the same spin polarization that electrical measurements alone cannot distinguish (*36*). In this setting, one would need to perform control experiments, such as changing the layer-stacking order or conducting thermal transport measurements. The situation is fundamentally different in antiferromagnets. The coexistence of both chiral modes in AF systems allows us to distinguish between coherent and incoherent contributions from the electrical measurements alone. The high-frequency (395 GHz) data for sample 3 in Fig. 2, A and B (see analogous data for sample 2 in fig. S1 and related discussion) indicate that electric signals from the HFM and LFM resonances (at $H = \pm 4.7$ T) behave in exact opposite ways when switching handedness. The HFM signal appears only at positive (negative) fields with the right-handed (left-handed) irradiation (*37*), as it corresponds to the right-handed (left-handed) chirality of the excited AF mode. In contrast, the sign of the spin Seebeck effect would be independent of the microwave handedness, because it primarily originates from the LFM mode (thermally more populated than the HFM) even if the microwave heating stems from the resonant absorption of microwave energy by the HFM. Because different frequencies need to be applied to excite the LFM and HFM, and a magnetic field is present, it is possible that the absorption of electromagnetic energy differs for each mode or polarization, causing different heating patterns (i.e., different spin Seebeck signals). Although this could account for the observed modulation of the ISHE signals of the two modes, such incoherent thermal effect cannot explain the complete reversal of the ISHE sign. Therefore, our experimental observation demonstrates unequivocally that the effect originates from coherent spin pumping and the ISHE in Pt.

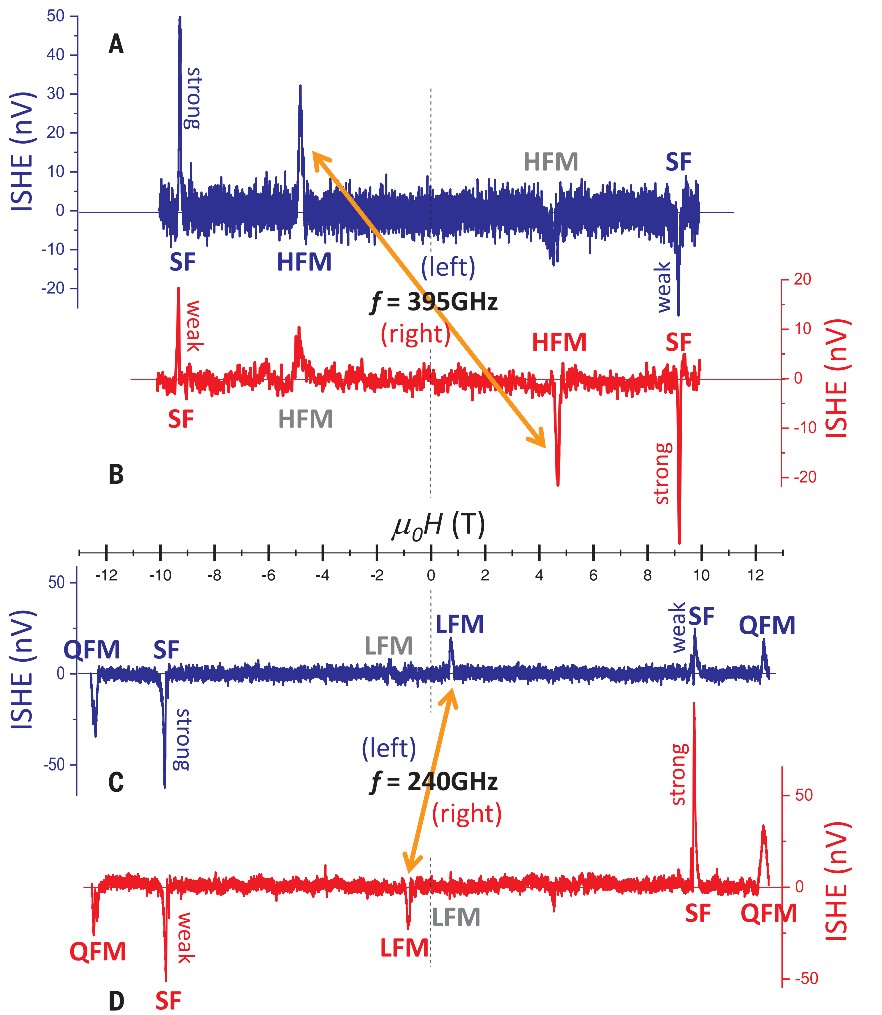

Fig. 2. Inverse spin Hall effect in MnF_2/Pt. ISHE signal obtained in MnF_2/Pt for sample 3 at f = 395 GHz (**A**) left- and (**B**) right-handed circularly polarized microwaves and for sample 2 at f = 240 GHz microwaves with both (**C**) left- and (**D**) right-handed circular polarization. A monotonous signal background has been subtracted from all spectra (*26*). Three distinct features are observed at 240 GHz: The LFM at $\mu_0 H = \pm 0.8$ T, the SF transition resonance at $\mu_0 H = \pm 9.73$ T, and the QFM resonance at $\mu_0 H = \pm 12.37$ T. Only the HFM and the SF resonances are observable for 395 GHz at $\mu_0 H = \pm 4.70$ and ± 9.15 T, respectively, within the available field range.

Given the coherent origin of the signals, we can further estimate the spin-mixing conductance of the MnF_2/Pt interface from the measured ISHE voltage. Taking into account the backflow of spin current in the Pt layer (with the spin-mixing conductance g_r in units of e^2/h per area, where e is electron charge and h is Planck's constant), we obtain (*4*, *19*)

$$V_{\mathrm{ISHE}} = L\theta_S \left(\frac{H_A}{H_E}\right)\left(\frac{\lambda}{d_N}\right)\frac{\hbar e(\gamma B_\perp)^2}{\alpha^2\omega_R}\frac{g_r \tanh\frac{d_N}{2\lambda}}{h\sigma + 2\lambda e^2 g_r \coth\frac{d_N}{2\lambda}} \quad (4)$$

where L is the distance between the two voltage leads; $d_N, \theta_S, \lambda, \sigma$ are the thickness, spin Hall angle, spin diffusion length, and conductivity of the Pt layer; α is the Gilbert damping in MnF_2, ω_R is the angular frequency of AFMR, $B_\perp$ is the amplitude of magnetic field of the circularly polarized microwave; and $\hbar = h/2\pi$ is the reduced Planck's constant. Even though it is difficult to acquire the exact value of every parameter, we can estimate the amplitude of g_r from data reported in the literature. In the MnF_2, we have $\frac{H_A}{H_E} \approx 1.8\%$ and $\alpha \approx 0.5 \times 10^{-3}$; in the Pt layer, $d_N \approx 4$ nm, $\theta_S \approx 0.08$, $\lambda \approx 1.4$ nm, and $\sigma \approx 4 \times 10^6$S/m (*38*, *39*). On the peak (dip) point of the 240-GHz resonance, $B_\perp \approx 200$ mG and $V_{\mathrm{ISHE}} \approx 25$ nV. Therefore, we obtain $g_r \approx 2.86 \times 10^{18}$ m^{-2}, which converts into $\approx 0.66\ e^2/h$ per unit cell area on the interface. This value, though a rough estimate owing to uncertainty in some of the parameters, is consistent with the theoretical prediction ($\approx 1\ e^2/h$) (*19*, *32*). Note that the extracted spin-mixing conductance is of a similar magnitude to that in ferromagnet or normal metal heterostructures, which confirms the theoretical prediction that opposite sublattice magnetizations can constructively pump, not cancel, spins.

Spin-flop mode and the high–magnetic field quasi-ferromagnetic mode

Now we consider the behavior of the SF and QFM signals. Although the handedness of the microwave polarization modulates the SF resonances, it does not substantially affect the QFM signal. The strength of the intermediate SF resonances, as shown in Fig. 2, is more pronounced when the polarization is right-handed (left-handed) for positive (negative) fields, which is the case for both frequencies. To highlight this result, Fig. 3 shows all ISHE signals as functions of the relative phase that determines the circular polarization of the microwaves. Whereas in the low-field regime ($H < H_{SF}$) both the LFM and the HFM exhibit oscillatory patterns as a function of the polarization phase (e.g., LFM feature in Fig. 3K), in the high-field regime ($H > H_{SF}$) the QFM signal is essentially constant (e.g., QFM feature in Fig. 3L). On the other hand, the SF signals display a mixture of both regimes—they oscillate on top of a constant background signal that has a similar magnitude to the 240-GHz QFM (red arrow in Fig. 3L). The appearance of phase modulation in the SF resonances is not surprising, as they partially retain the features (especially the chirality) of the HFM, whereas the ground state undergoes a gradual evolution from the colinear configuration into the SF configuration. However, the sign of the 395-GHz SF resonance is opposite that of the 240-GHz resonance and requires a more detailed analysis.

In Fig. 4A, we directly compare the phase-modulation pattern for four particular resonances under positive magnetic fields; Fig. 4B relates them to four representative points on the upper-frequency branch and illustrates their physical meaning. In the low-field regime, as described by point 1, the nonequilibrium (dynamical) spin angular momentum m_d carried by the HFM opposes the magnetic field. In the high-field regime, once the sublattice magnetizations have flopped into a direction perpendicular to the applied magnetic field, as depicted by point 4, a finite (static) magnetization m_s along the magnetic field is induced in the ground state because the Zeeman interaction cants both sublattices toward the applied field. The QFM refers to a right-handed rotation of the induced magnetization m_s, similar to a ferromagnet (*21*), which is why it is named QFM; the sublattice magnetizations are still strongly antiferromagnetically connected by the predominant exchange interaction. Correspondingly, the nonequilibrium spin angular

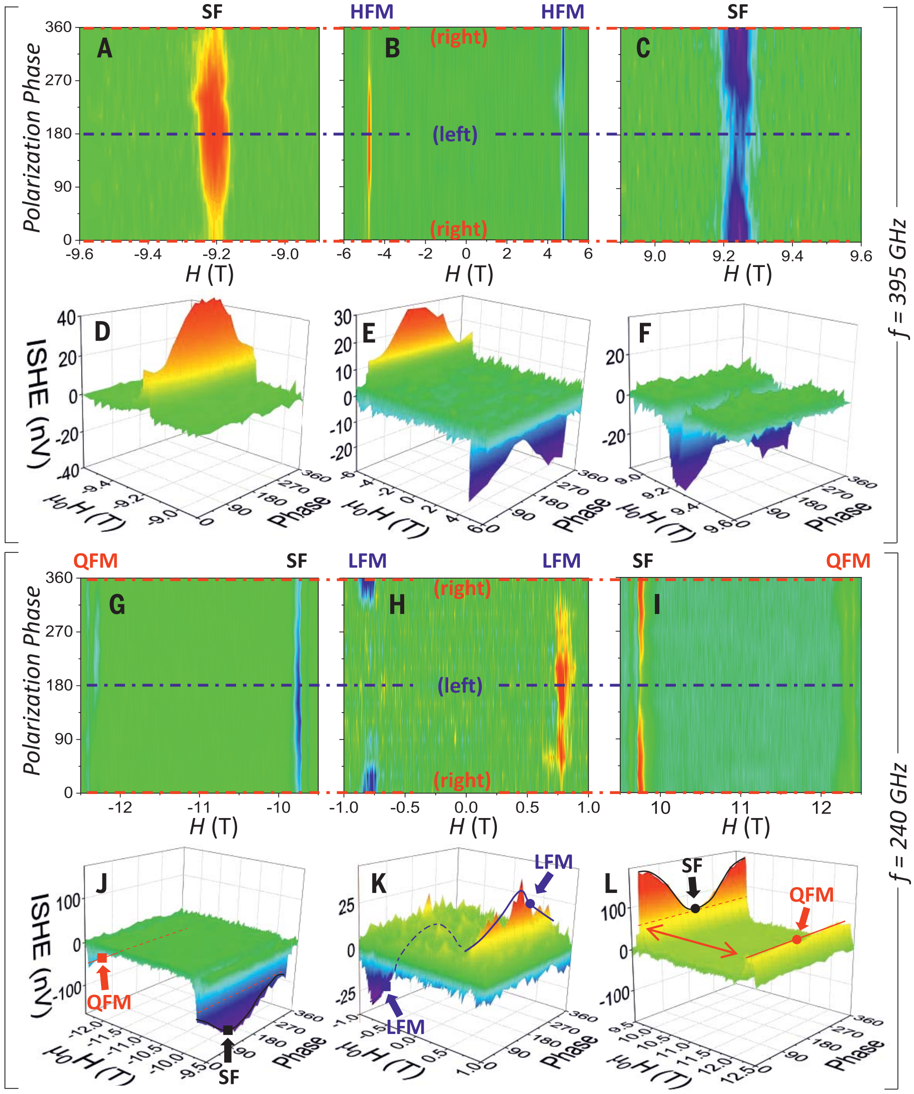

Fig. 3. Circular polarization modulation of spin pumping. Evolution of the ISHE signals (magnitude given in the 3D plots) with magnetic field as a function of the polarization of the subterahertz microwaves for (**A** to **F**) f = 395 GHz and (**G** to **L**) 240 GHz. Left-handed (right-handed) circular polarization is achieved at 180° (0°, 360°).

momentum m_d induced upon excitation is negative with respect to the magnetic field; its sign follows that of the HFM. However, the measured ISHE signal arising from the QFM does not follow this rule, indicating that the spin current may not be originating from coherent spin pumping at point 4. As a theoretical check, we numerically calculated the dc coherent spin pumping for all points given by the following expression (*19*)

$$\frac{e}{\hbar}\vec{I}_s = G_r(\vec{n}\times\dot{\vec{n}} + \vec{m}\times\dot{\vec{m}}) - G_i\dot{\vec{m}} \qquad (5)$$

where $G_r = g_r e^2/h$ is the mixing conductance extracted from Eq. 4. Note that the last term averages to zero on a magnetization precession cycle and thus does not contribute to dc spin pumping. The corresponding calculated ISHE voltages generated by the pumped spins are shown in Fig. 4A (lines). Theory can quantitatively account for the behavior of the HFM (point 1 in Fig. 4A); however, it fails to explain the SF and the QFM signals. For the upper-frequency branch, the theory predicts the same polarization modulation and sign for all ISHE signals arising from coherent spin pumping, with varying magnitudes for the different points. Figure S6 shows the calculated trajectories of the sublattice magnetizations corresponding to points 1 to 4 in Fig. 4; sublattice magnetization with overall projection along the applied field displays a larger precession angle than its opposite, resulting in a dynamical net moment against the applied field in all cases (i.e., negative ISHE voltage). Experimentally, the 395-GHz SF signal exhibits the expected

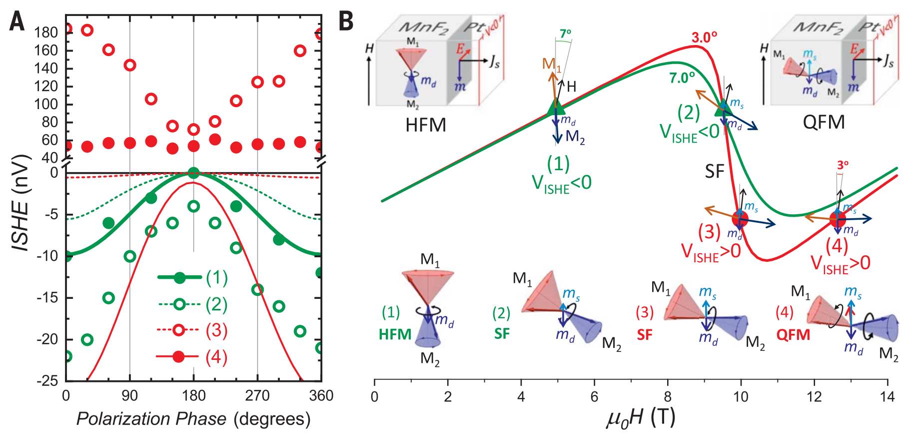

Fig. 4. Evolution of spin dynamics across the SF transition. (**A**) ISHE signals of the 395-GHz HFM (point 1), 395-GHz SF (point 2), 240-GHz SF (point 3), and 240-GHz QFM (point 4). Experimental data (dots) and numerical simulation based on coherent spin pumping (curves) agree quantitatively for point 1 and qualitatively for point 2; points 3 and 4 cannot be captured by coherent spin pumping. We used a larger microwave power in the 240-GHz resonances—hence the larger magnitude of the signals for points 3 and 4. (**B**) Illustration of the orientations of the sublattice magnetizations $\vec{M}_1$ and $\vec{M}_2$ and the applied field H_0 (with H_A along the vertical z axis) for four resonances (1 and 2 for 395 GHz and 3 and 4 for 240 GHz) representative of the change in AF dynamics in transiting from the HFM into the QFM through the SF region. The upper sketches represent the orientation and spin polarization of the pumped spin current and the induced ISHE electric field with respect to the measuring circuit in the sample. The lower insets illustrate the precessional cones of $\vec{M}_1$ and $\vec{M}_2$ for each of the resonances.

sign and polarization modulation but is substantially larger than expected from theory. The 240-GHz SF has the expected polarization modulation but not the sign. Finally, as mentioned above, the QFM exhibits neither the modulation nor the sign predicted by theory, confirming that coherent spin pumping is unlikely to be the mechanism behind the system response after the SF transition.

A possible explanation of the independence of the QFM signal on the microwave polarization is that the QFM signal arises from a combined effect of magnetic proximity and thermal spin-current generation. Specifically, it is possible that the ground-state magnetization polarizes the conduction electrons in the Pt so that most spins are parallel to the magnetization and, hence, to the applied magnetic field. At the QFM resonance, microwave heating leads to a temperature gradient in the thickness direction, which in turn generates a spin-polarized current in the Pt that converts into an ISHE voltage.

In the unusual regime of the SF transition, the spin dynamics gradually loses the HFM characteristic while acquiring the QFM behavior. In Fig. 4B, point 2 (point 3) marks the 395-GHz (240-GHz) SF resonance, where the sign of ISHE follows that of the HFM (QFM) at point 1 (point 4). This strongly suggests that there must be a turning point between points 2 and 3 at which the spin current starts to be dominated by the ground-state magnetization rather than the nonequilibrium spin angular momentum in MnF_2. However, the exact location of this critical point and how the eigenmodes evolve in the vicinity of this point can only be determined numerically in the presence of a finite misalignment angle. In fig. S5, we calculated the net equilibrium magnetization as a function of field, qualitatively verifying the above behavior.

By comparing Fig. 2 and Fig. 4 for the 240-GHz resonance, we further notice that the SF signal (point 3) is stronger than the QFM signal (point 4) even though the ground-state magnetization, and hence the proximity effect, is apparently smaller at point 3, as the QFM behavior there is not fully developed. A possible reason is that within the narrow window of SF transition, the ground state becomes highly unstable, which appreciably enlarges the dynamical susceptibility $\chi(\omega)$. Under fixed microwave power, the heat production rate is proportional to $|\chi(\omega)|^2$. Therefore, it is natural to expect a markedly larger heating effect at point 3 than at point 4. The subtle behavior in the vicinity of SF transition calls for further systematic measurements with additional microwave frequencies.

Outlook

The demonstration of the coherent spin-pumping effect in MnF_2/Pt opens the door to advancements in controlling and understanding spin-transfer torques in AF-based systems that may lead to energy-efficient and fault-tolerant spintronic devices operating at terahertz frequencies. Further exploration of spin pumping in AF-based systems will enable a thorough understanding of the relation between the structural symmetries of antiferromagnets, the characteristics of their spin dynamics, and the polarization of the associated terahertz signals, which will aid the design of next-generation spintronic applications in which antiferromagnets are active players.

REFERENCES AND NOTES

1. L. Néel, *Ann. Phys.* **11**, 232–279 (1936).
2. P. Wadley *et al.*, *Science* **351**, 587–590 (2016).
3. D. Kriegner *et al.*, *Nat. Commun.* **7**, 11623 (2016).
4. R. Cheng, D. Xiao, A. Brataas, *Phys. Rev. Lett.* **116**, 207603 (2016).
5. R. Khymyn, I. Lisenkov, V. Tiberkevich, B. A. Ivanov, A. Slavin, *Sci. Rep.* **7**, 43705 (2017).
6. R. Khymyn, I. Lisenkov, V. S. Tiberkevich, A. N. Slavin, B. A. Ivanov, *Phys. Rev. B* **93**, 224421 (2016).
7. R. Kleiner, *Science* **318**, 1254–1255 (2007).
8. J. Nogués, I. K. Schuller, *J. Magn. Magn. Mater.* **192**, 203–232 (1999).
9. B. G. Park *et al.*, *Nat. Mater.* **10**, 347–351 (2011).
10. Y. Y. Wang *et al.*, *Phys. Rev. Lett.* **109**, 137201 (2012).
11. X. Marti *et al.*, *Nat. Mater.* **13**, 367–374 (2014).
12. I. Fina *et al.*, *Nat. Commun.* **5**, 4671 (2014).
13. S. Y. Bodnar *et al.*, *Nat. Commun.* **9**, 348 (2018).
14. M. Meinert, D. Graulich, T. Matalla-Wagner, *Phys. Rev. Appl.* **9**, 064040 (2018).
15. J. Železný *et al.*, *Phys. Rev. Lett.* **113**, 157201 (2014).
16. R. Lebrun *et al.*, *Nature* **561**, 222–225 (2018).
17. A. S. Núñez, R. Duine, P. Haney, A. MacDonald, *Phys. Rev. B* **73**, 214426 (2006).
18. H. V. Gomonay, V. M. Loktev, *Phys. Rev. B* **81**, 144427 (2010).
19. R. Cheng, J. Xiao, Q. Niu, A. Brataas, *Phys. Rev. Lett.* **113**, 057601 (2014).
20. P. Ross *et al.*, *J. Appl. Phys.* **118**, 233907 (2015).
21. C. Kittel, *Phys. Rev.* **82**, 565 (1951).
22. T. Nagamiya, K. Yosida, R. Kubo, *Adv. Phys.* **4**, 1–112 (1955).
23. There is an additional zero-energy mode (spin-superfluid mode) after the SF transition. This mode becomes visible only at low frequencies when the field is applied away from the easy anisotropy axis, but this mode is not accessible within our range of frequencies and will not be further discussed in this work.
24. J. Kotthaus, V. Jaccarino, *Phys. Rev. Lett.* **28**, 1649–1652 (1972).
25. M. Hagiwara *et al.*, *Int. J. Infrared Millim. Waves* **20**, 617–622 (1999).
26. A detailed discussion is presented in supplementary text section S1: "Spectroscopy and ISHE Measurements."
27. I. S. Jacobs, *J. Appl. Phys.* **32**, S61–S62 (1961).
28. Y. Tserkovnyak, A. Brataas, G. E. Bauer, *Phys. Rev. Lett.* **88**, 117601 (2002).
29. A. Brataas, Y. Tserkovnyak, G. E. Bauer, B. I. Halperin, *Phys. Rev. B* **66**, 060404 (2002).
30. Y. Tserkovnyak, A. Brataas, G. E. Bauer, *Phys. Rev. B* **66**, 224403 (2002).
31. E. Saitoh, M. Ueda, H. Miyajima, G. Tatara, *Appl. Phys. Lett.* **88**, 182509 (2006).
32. Ø. Johansen, A. Brataas, *Phys. Rev. B* **95**, 220408 (2017).
33. R. Cheng, thesis, The University of Texas at Austin (2014).
34. S. M. Rezende, R. L. Rodríguez-Suárez, A. Azevedo, *Phys. Rev. B* **93**, 014425 (2016).
35. S. M. Wu *et al.*, *Phys. Rev. Lett.* **116**, 097204 (2016).
36. W. Lin, C. L. Chien, arXiv:1804.01392 [cond-mat.mtrl-sci] (28 Mar 2018).
37. The presence of the sample prevents the achievement of perfect circular polarization, which results in a small residual ISHE signal that varies with the size of the sample.
38. L. Liu, R. A. Buhrman, D. C. Ralph, arXiv:1111.3702 [cond-mat.mes-hall] (16 Nov 2011).
39. W. Zhang *et al.*, *Appl. Phys. Lett.* **103**, 242414 (2013).
40. P. Vaidya, Sub-Terahertz Spin Pumping from an Insulating Antiferromagnet, Version 1.0, Harvard Dataverse (2020); https://doi.org/10.7910/DVN/RFCH1Q.

ACKNOWLEDGMENTS

We thank A. Ramirez of the Materials Advancement Portal at UC Santa Cruz (https://materials.soe.ucsc.edu/home) for providing the MnF_2 single crystal. **Funding:** P.V., R.C., D.L., and E.d.B. acknowledge support from the Air Force Office of Scientific Research under grant FA9550-19-1-0307. A.B. acknowledges support from the European Research Council via Advanced Grant 669442 "Insulatronics" and the Research Council of Norway via project 262633 "QuSpin." The work at UC Santa Cruz was supported in part by the University of California Multicampus Research Programs and Initiatives grant MRP-17-454963. A portion of this work was performed at the National High Magnetic Field Laboratory, which is supported by the National Science Foundation Cooperative Agreement DMR-1644779 and the state of Florida. **Author contributions:** P.V., S.A.M., J.v.T., D.L., and E.d.B, conceived and designed the experiments. P.V. and J.v.T performed the high-frequency experiments. S.A.M. performed the materials characterization experiments. S.A.M. and D.L. provided the samples. P.V. and E.d.B analyzed the data and performed numerical simulations. Y.L. and R.C. computed the dynamical response of the system and the corresponding spin pumping. A.B. suggested the experimental detection. Both R.C. and A.B. assisted with the theoretical interpretations of the results. All authors contributed to discussions and manuscript writing. **Competing interests:** The authors declare no competing interests. **Data and materials availability:** All data in the main text and the supplementary materials, along with the code used to analyze the data and generate the fitted plots, are available at the Harvard Dataverse (*40*).

SUPPLEMENTARY MATERIALS

science.sciencemag.org/content/368/6487/160/suppl/DC1
Materials and Methods
Supplementary Text
Figs. S1 to S7
References (*41*, *42*)
Movies S1 to S4

9 September 2019; accepted 12 March 2020
10.1126/science.aaz4247

Science

Subterahertz spin pumping from an insulating antiferromagnet

Priyanka Vaidya, Sophie A. Morley, Johan van Tol, Yan Liu, Ran Cheng, Arne Brataas, David Lederman and Enrique del Barco

Science **368** (6487), 160-165.
DOI: 10.1126/science.aaz4247

A spin-pumping antiferromagnet

Antiferromagnets have been used in spintronics mainly as a source of the so-called exchange bias. However, they hold promise for a much more active role given that their magnetization dynamics can in principle be much faster than those in ferromagnets. For this promise to materialize, antiferromagnets must learn the tricks that come naturally to ferromagnets. Vaidya *et al.* observed one such phenomenon called spin pumping (see the Perspective by Hoffmann). The researchers irradiated the antiferromagnet MnF_2 with circularly polarized subterahertz light, causing the spins in this material to spring into action. These dynamics, in turn, caused the injection of spin current into a layer of platinum adjacent to MnF_2.

Science, this issue p. 160; see also p. 135

Science (print ISSN 0036-8075; online ISSN 1095-9203) is published by the American Association for the Advancement of Science, 1200 New York Avenue NW, Washington, DC 20005. The title *Science* is a registered trademark of AAAS.